Supporting Information

Defective g-C_3N_4/RGO/TiO_2 composite from hydrogen treatment for enhanced visible-light photocatalytic H_2 production

Jing Wang [a], Youcai Sun [b], Lijun Fu [a], Zhuang Sun [c], Man Ou [a], Shulin Zhao [a], Yuhui Chen [a], Fengjiao Yu [b*], and Yuping Wu [a*]

[a.] *School of Energy Science and Engineering, Nanjing Tech University. Nanjing, Jiangsu, 211816, China*

[b.] *College of Chemical Engineering, Nanjing Tech University. Nanjing, Jiangsu, 211816, China*

[c.] *State Key Lab of High Performance Ceramics and Superfine Microstructure, Shanghai Institute of Ceramics, Chinese Academy of Sciences, Shanghai, 200050, China*

Email: wuyp@fudan.edu.cn; fjyu@njtech.edu.cn

Experimental sections

Preparation of g-C_3N_4 material

Melamine and ammonium chloride in this study were analytical grade and used without further purification. Typically, melamine was calcined at 520 ℃ for 4 h (a heating ramp of 5 ℃ min^{-1}). The resulting yellow agglomerate, bulk g-C_3N_4, was ground into powders (denoted as BCN). After that, BCN powders and ammonium chloride were ground together in an agate mortar to make homogeneous mixture in a weight ratio of 5:1, then transferred the mixture into a crucible and calcined at the temperature of 550 ℃ for 3 h with a heating ramp of 3 ℃ min^{-1} in air. The obtained yellow sample was g-C_3N_4 sheets.

Synthesis of CGT and CGT-H_2 samples

In a typical synthesis procedure of CGT sample, 0.1 g g-C_3N_4 sheets were dispersed in 100 mL of methanol, and then 10 mg of commercial TiO_2 nanoparticles and 6 mg ml^{-1} of graphene oxide (GO) were added to obtain a homogeneous suspension. After reflux for 5 h at 80 ℃, GO reacted with methanol to form reduced graphene oxide (RGO), and the evaluated mass fraction of RGO was approximately 0.2 wt.%. The resulting product was g-C_3N_4/RGO/TiO_2 (CGT). Subsequently, CGT sample was transferred into a quartz boat and calcined at 500 ℃ for 1 h at a ramping rate of 2 ℃ min^{-1} in flowing Ar/H_2 (95/5 v/v) atmosphere to obtain defective g-C_3N_4/RGO/TiO_2 (CGT-H_2). In typical CGT-H_2, the mass fraction of RGO and TiO_2 was 0.2

wt.% and 10 wt.%, respectively. Different defective samples were prepared by varying the mass fraction of TiO_2 in composite (x wt.%), denoted as CGT-H_2 (x), where x = 0, 5, 10, 15 and 20. In addition, g-C_3N_4-H_2, TiO_2-H_2, g-C_3N_4/TiO_2-H_2 (CT-H_2), and RGO/TiO_2-H_2 (GT-H_2) were prepared by treating g-C_3N_4, TiO_2, g-C_3N_4/TiO_2, and RGO/TiO_2 at 500 ℃ (2 ℃ min^{-1}) for 1 h in flowing Ar/H_2 (95/5 v/v).

Characterization

The morphology was characterized by high-resolution transmission electron microscopy (JEM-2100 plus, JEOL Co.) with an accelerating voltage of 200 kV. Powder X-ray diffraction (XRD) patterns were taken in the range of 10-90^o (2θ) using a Rigaku Smartlab instrument with Cu K_α-source (λ = 1.5418 Å). The diffuse reflectance spectra over the range of 200-800 nm were measured on an ultraviolet-visible spectrophotometer with a Labsphere diffuse reflectance accessory (UV 2600, Shimadzu Co.). Nitrogen adsorption and desorption measurements were performed with an Autosorb iQ instrument, the surface areas were calculated by Brunauer-Emmett-Teller (BET) method. The chemical compositions were characterized using a Kratos AXIS Ultra DLD X-ray photoelectron spectrometer. Raman spectra were recorded on a Raman microscope (LABRAM-HR, JY Co.). Photoluminescence (PL) spectra were collected on an Edinburgh spectrofluorometer (FLS980) with an excitation wavelength of 380 nm from a Xenon lamp. The transient photocurrent response of as-prepared samples was conducted on a three-electrode set-up (CHI 660D potentiostat), where a sample-coated on fluoride-tin oxide (FTO) glass, a saturated calomel electrode (SCE), and a Pt wire were used as the working electrode, reference electrode, and counter electrode, respectively. The aqueous solution of 0.2 M Na_2SO_4 purged with nitrogen was chosen to be the electrolyte. A 300 W Xenon lamp with a 400 nm cutoff filter was used as a light source. The electrochemical impedance spectroscopy (EIS) measurement was carried out in the frequency range of 10^{-2} to 10^5 Hz with an AC voltage amplitude of 10 mV at a DC bias of 1.8 V_{SCE} in a dark circumstance.

Photocatalytic H_2 evolution measurements

The performance of photocatalytic H_2 production was evaluated using an online photocatalytic H_2 generation system (Labsolar-6A). A 300 W Xe lamp (CEL-HX300) equipping with a UV cut 400 filter was used as the visible light source. In a typical test, 10 mg of photocatalyst was dispersed in 80 mL of aqueous solution containing 10 vol.% of triethanolamine (TEOA). 2 wt.% Pt, a co-catalyst, was photo-deposited uniformly on the surface of as-synthesized photocatalysts using K_2PtCl_6 as the precursor. Prior to irradiation, the dissolved air in suspension was degassed thoroughly by an evacuation system. The whole photocatalytic procedure was performed at 6 ℃ under visible-light irradiation by adopting a liquid trap system with water circulation. After a photo-depositing period of 30 min, the amount of H_2 evolution was quantitatively analyzed by a FULI 979011 gas chromatography with a TCD detector online.

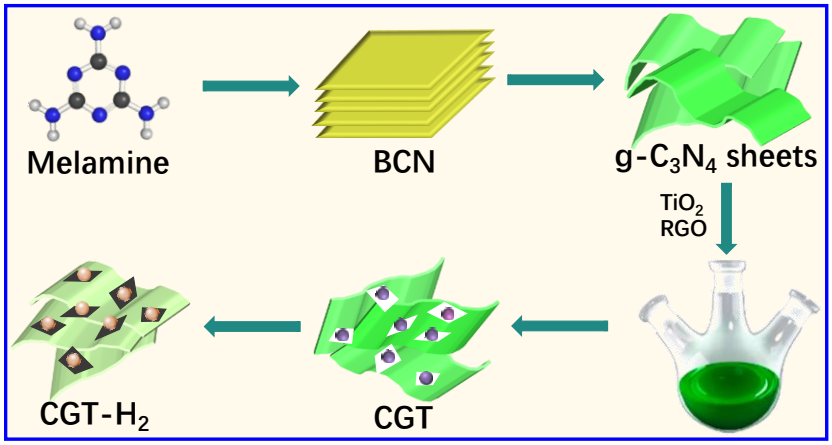

Fig. S1 Schematic procedures for preparing CGT and CGT-H_2 samples.

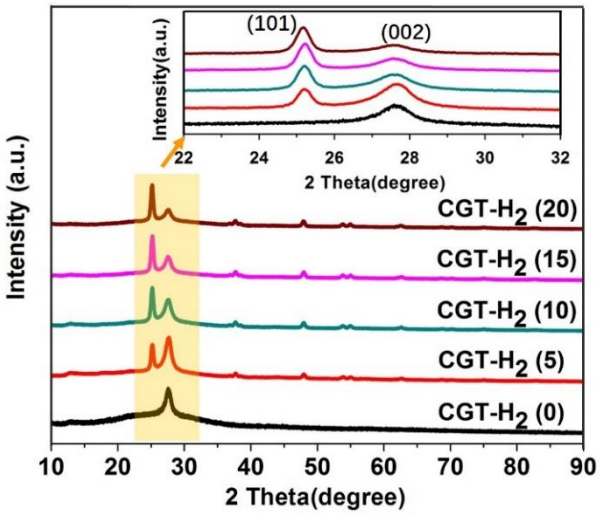

Fig. S2 XRD patterns of CGT-H_2 (0), CGT-H_2 (5), CGT-H_2 (10), CGT-H_2 (15), CGT-H_2 (20) samples, and inset is the enlarged XRD spectra in the range of 22-32^o (2θ).

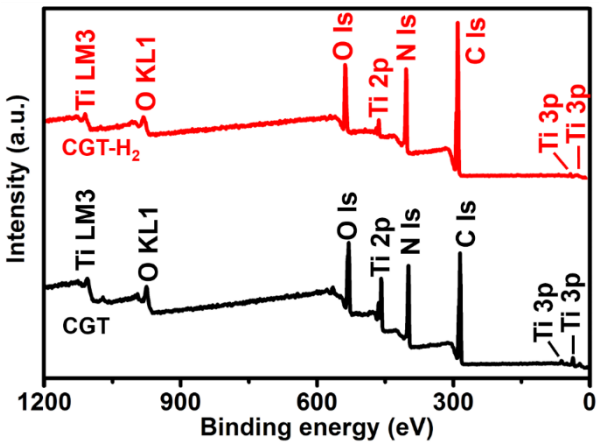

Fig. S3 Survey XPS spectra of CGT-H_2 and CGT samples, respectively.

.

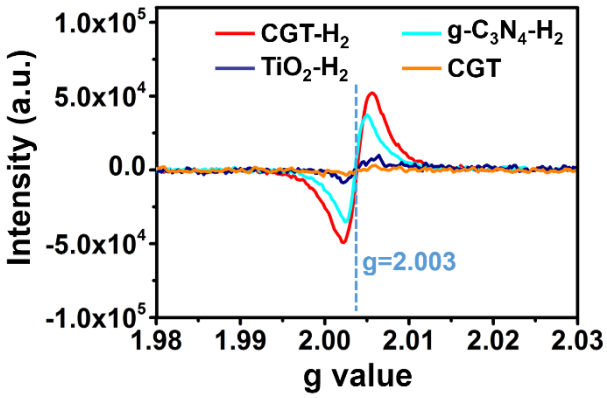

Fig. S4 EPR Spectra of CGT-H_2, g-C_3N_4-H_2, TiO_2-H_2, and CGT samples.

g-C_3N_4 and TiO_2 were thermal treated at 500 °C for 1 h at a ramping rate of 2 °C min^{-1} in flowing Ar/H_2 (95/5 v/v) atmosphere separately, and named them as g-C_3N_4-H_2 and TiO_2-H_2, respectively. The EPR curves (Fig.S4) illustrate that g-C_3N_4-H_2 and TiO_2-H_2 have the similar g value of CGT-H_2 (2.003), which suggests nitrogen vacancies and oxygen vacancies are separately introduced in g-C_3N_4 and TiO_2 through hydrogen treatment.

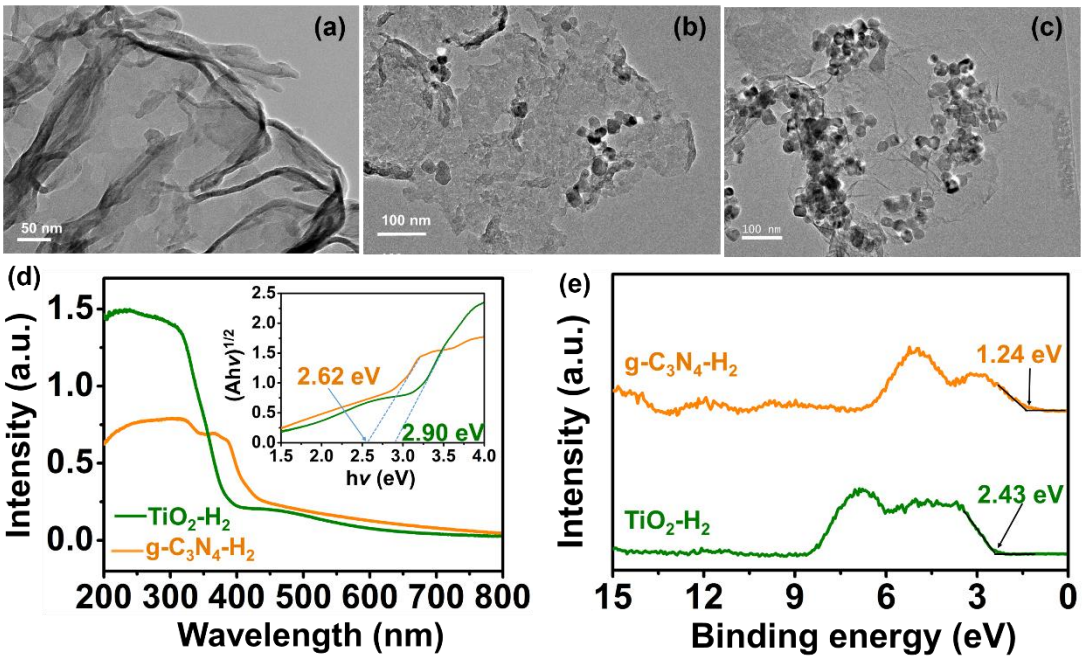

Fig. S5 (a-c) TEM images of g-C_3N_4-H_2, g-C_3N_4/TiO_2-H_2 (CT-H_2), RGO/TiO_2-H_2 (GT-H_2) samples; (d) UV-vis diffuse reflectance spectra (UV-DRS) of g-C_3N_4-H_2 and TiO_2-H_2 (inset is the according band gap); (e) The valence band X-ray photoelectron spectroscopy (VB-XPS) of g-C_3N_4-H_2 and TiO_2-H_2.

In Fig. S5a-d, g-C_3N_4-H_2 displays a large sheet structure; TiO_2 nanoparticles can be successfully deposited not only on the surface of the g-C_3N_4 sheets in g-C_3N_4/TiO_2-H_2 (CT-H_2, Fig. S5b), but also on the RGO surface in RGO/TiO_2-H_2 (GT-H_2, Fig. S5c). Based on the band position of g-C_3N_4-H_2 and TiO_2-H_2 (Fig. 2e), we first excluded the Z-scheme system. The heterojunction is therefore a type II with two possible transfer routes. The first route is that the photogenerated electrons transfer from the CB of g-C_3N_4-H_2 to the CB of TiO_2-H_2, and then to RGO. In this case, Pt must be deposited on the surface of RGO to reduce H^+ to H_2. The second is that the photogenerated electrons in the CB of g-C_3N_4-H_2 transfer to RGO and then to the CB of TiO_2-H_2. In this case, Pt must be deposited on the TiO_2-H_2 surface to reduce H^+ to H_2. As seen in Fig 2c-d, Pt nanoparticles are photodeposited on the TiO_2 surface. This confirms that the charge transfer route is the second one. To be precise, the photogenerated electrons transfer from g-C_3N_4 to TiO_2 through RGO and are then directed to Pt before finally reducing H^+ to H_2. Therefore, the heterojunction mode of CGT-H_2 can be proposed as 2D-2D-0D as in Fig. 2f.

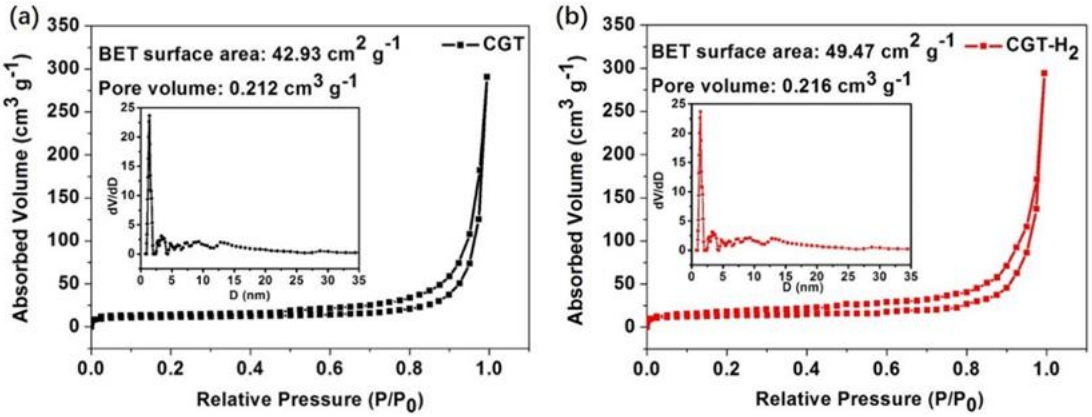

Fig. S6 N_2 adsorption-desorption isotherms and the pore size distribution plots (inset). (a) CGT and (b) CGT-H_2 sample.

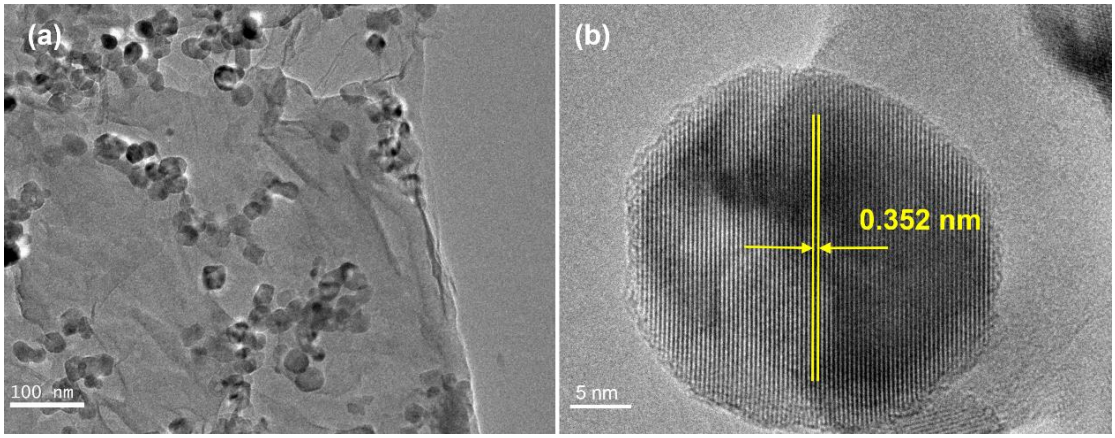

Fig. S7 (a) TEM and (b) HRTEM images of CGT sample.

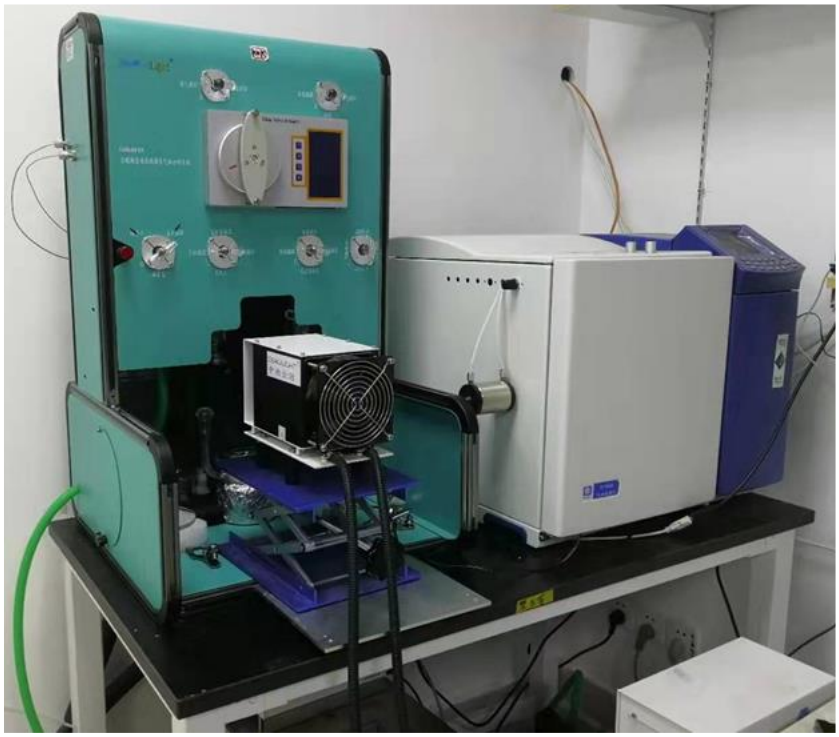

Fig. S8 Photograph of an online photocatalytic test system.

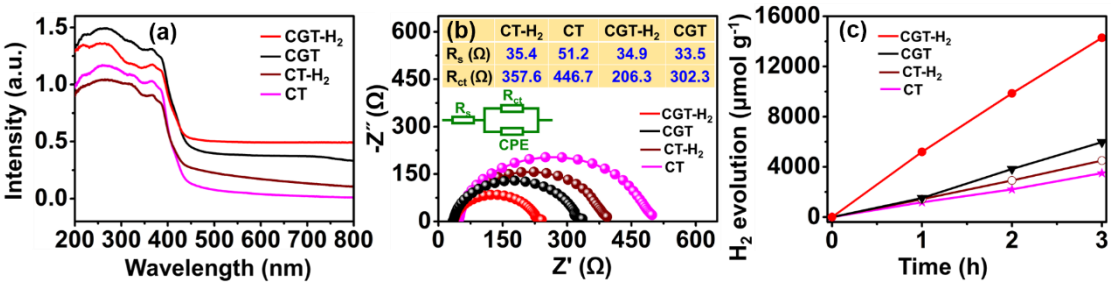

Fig. S9 (a, b, c) UV-DRS, EIS, and H_2 evolution performance of CT, CT-H_2, CGT, and CGT-H_2, respectively.

In Fig. S9, all of the UV-DRS, EIS, and H_2 evolution performance of CT, CT-H_2, CGT, and CGT-H_2 display obvious differences. We can observe the stronger light absorption and the smaller Rct, as well as more H_2 evolution amount of CGT and CGT-H_2 than those of CT and CT-H_2 samples.

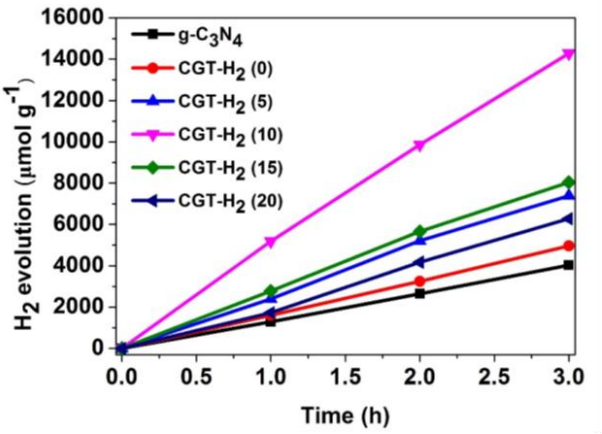

Fig. S10 The time-dependent photoinduced H_2 evolution over g-C_3N_4, CGT-H_2 (0), CGT-H_2 (5), CGT-H_2 (10), CGT-H_2 (15), and CGT-H_2 (20) samples loaded with 0.2% RGO and various amount of TiO_2 under visible light irradiation (λ > 400 nm) in 80 ml of 10 vol.% of TEOA aqueous solution.

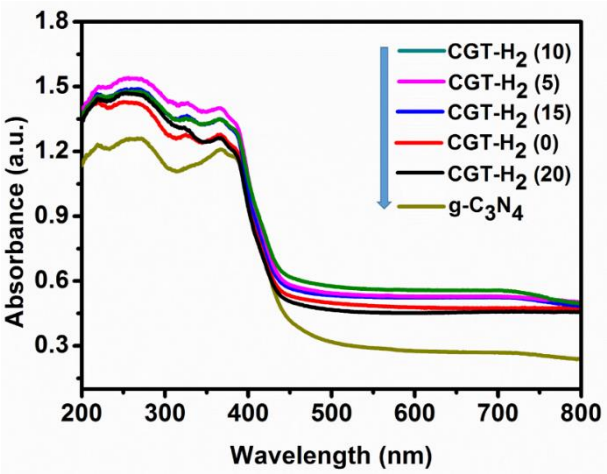

Fig. S11 UV-vis diffuse reflectance spectra of g-C_3N_4, CGT-H_2 (0), CGT-H_2 (5), CGT-H_2 (10), CGT-H_2 (15), and CGT-H_2 (20) samples.

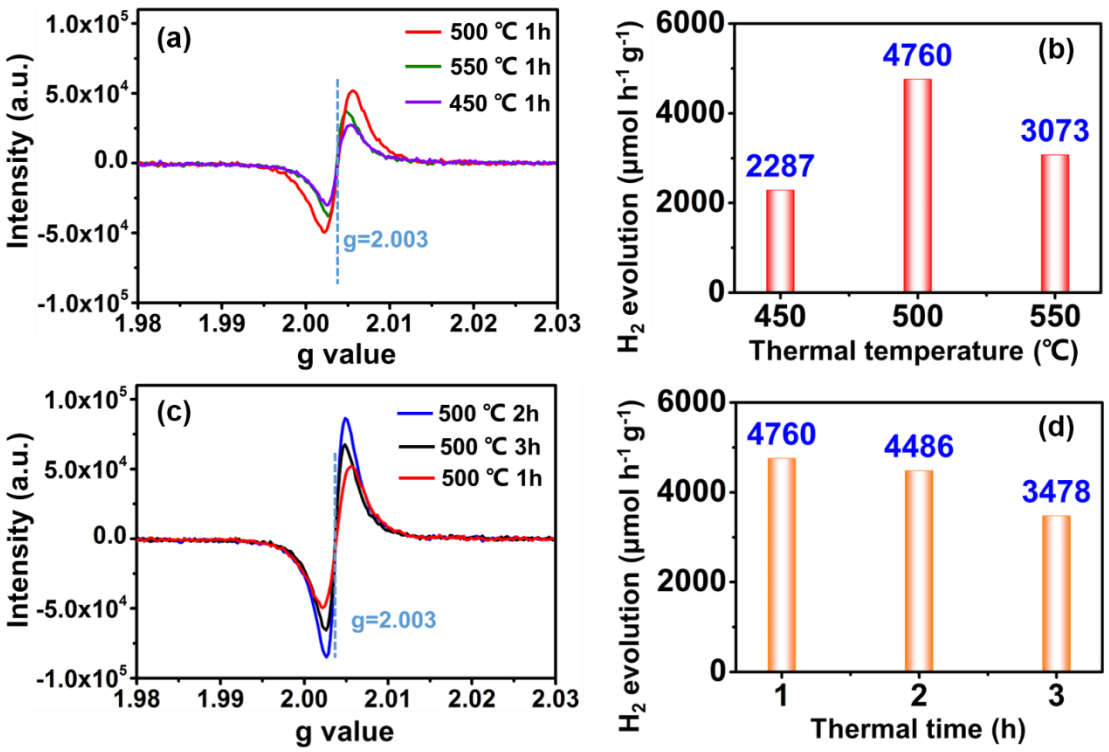

Fig. S12 EPR and H_2 evolution rate of various sampels. (a-b) CGT was hydrogen treated at 450, 500, and 550 ℃ for 1h, respectively; (c-d) CGT was hydrogen treated at 500 550 ℃ for 1h, 2h, and 3h, respectively.

The EPR and photocatalytic activities of various samples were shown in Fig. S12. In contrast, we found that the amount of defects changed in accordance with hydrogen-treatment time and temperature. However, H_2 production is not overly high when the amount of defects is too high or too low. The photocatalytic activity of the sample that was hydrogen treated at 500 ℃ for one hour is the highest, and the resulting amount of defects in the sample is optimal.

Table S1 Elemental analyzer (EA) and XPS results for CGT and CGT-H_2.

	EA (element mass ratios)					XPS (atomic ratios)				
Samples	C	N	O	N/C	O/C	C	N	O	N/C	O/C
CGT	30.19	53.49	27.282	1.772	0.904	34.31	44.52	8.31	1.298	0.242
CGT-H_2	30.18	52.68	13.882	1.746	0.460	42.89	47.57	5.66	1.109	0.132

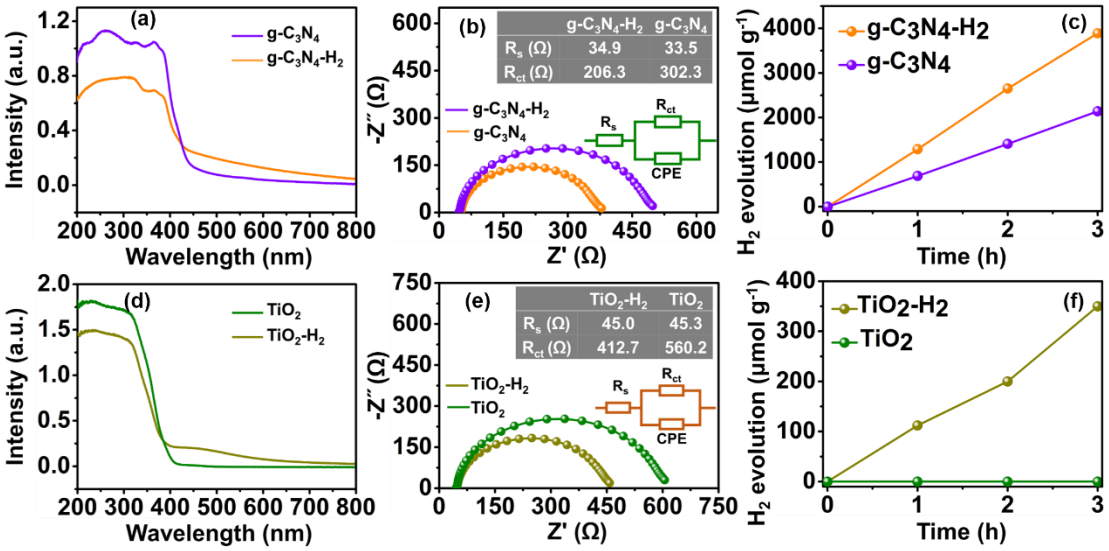

Fig. S13 UV-DRS, EIS, and H_2 evolution amount of various samples. (a-c) g-C_3N_4 and g-C_3N_4-H_2; (d-f) TiO_2 and TiO_2-H_2.

Notable changes are observed between g-C_3N_4 and g-C_3N_4-H_2 in Fig. S13a-c. Specifically, visible absorption is enhanced, charge transfer resistance is decreased, and H_2 evolution activity is boosted. In Fig. S13d-f, for TiO_2, light absorption from 400-600 nm is improved, charge transfer resistance is decreased, and the H_2 evolution activity is notably enhanced after introducing oxygen defects through hydrogen treatment. Therefore, both nitrogen and oxygen defects affect the performance of CGT-H_2 in terms of visible absorption and charge-transfer efficiency individually.

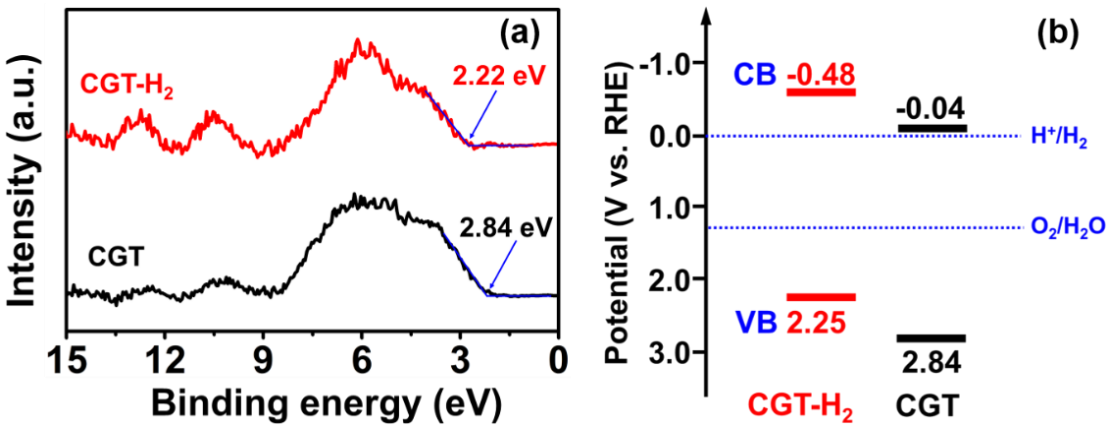

Fig. S14 (a) The valence band X-ray photoelectron spectroscopy (VB-XPS); (b) Band structure diagram for CGT and CGT-H_2.

`

Table S2 Comparison of the H_2 production rate for representative photocatalysts.

Photocatalyst	Light type	Sacrificial reagent	H_2 evolution rate	Reference
g-C_3N_4/TiO_2	350 W Xe lamp	TEOA	4128 μmol h^{-1} g^{-1}	1
g-C_3N_4/B-TiO_2	λ > 400 nm 300 W Xe Lamp	Methanol	47.3 μmol h^{-1} g^{-1}	2
g-C_3N_4-TiO_2	λ ≥ 400 nm 300 W Xe lamp	TEOA	294 μmol h^{-1} g^{-1}	3
O-g-C_3N_4/TiO_2	λ > 400 nm 300 W Xe lamp	TEOA	566 μmol h^{-1} g^{-1}	4
g-C_3N_4/TiO_2	λ > 420 nm 300 W Xe lamp	TEOA	329 μmol h^{-1} g^{-1}	5
g-C_3N_4/TiO_2	500 W Xe lamp	Methanol	527 μmol h^{-1} g^{-1}	6
g-C_3N_4/TiO_2	λ= 200 - 800 nm 250 W Xe lamp	Glycerol	23143 μmol h^{-1} g^{-1}	7
g-C_3N_4/TiO_2	300 W Xe lamp	TEOA	1520 μmol h^{-1} g^{-1}	8
TiO_2-C_3N_4	250 W visible light	TEOA	1042 μmol h^{-1} g^{-1}	9
g-C_3N_4/TiO_2	300 W Xe lamp	TEOA	4660 μmol h^{-1} g^{-1}	10
g-C_3N_4/N-TiO_2	300 W Xe lamp	Methanol	8931 μmol h^{-1} g^{-1}	11
g-C_3N_4/TiO_2	λ > 400 nm 300 W Xe lamp	Methanol	1938 μmol h^{-1} g^{-1}	12
TiO_2@g-C_3N_4	Visible light	Methanol	198 μmol h^{-1} g^{-1}	13
g-C_3N_4/TiO_2	λ ≥ 420 nm 300 W Xe lamp	TEOA	1780 μmol h^{-1} g^{-1}	14
C-TiO_2/g-C_3N_4	λ ≥ 420 nm 300 W Xe lamp	TEOA	1409 μmol h^{-1} g^{-1}	15
g-C_3N_4/RGO/TiO_2 (CGT)	λ > 400 nm 300 W Xe lamp	TEOA	1987 μmol h^{-1} g^{-1}	***This work***
defective g-C_3N_4/RGO/TiO_2 (CGT-H_2)	λ > 400 nm 300 W Xe lamp	TEOA	4760 μmol h^{-1} g^{-1}	***This work***

Table S3 The comparison of EQE reported g-C_3N_4-based photocatalysts.

Photocatalyst	Reaction condition	EQE	Reference
Few-layer g-C_3N_4	1 wt% Pt co-catalyst 20% TEOA solution 20 mg catalyst	9.8% (420 nm)	16
C_{ring}-C_3N_4	Ultrapure water 3 wt% Pt co-catalyst 10 mg catalyst	5 % (420 nm)	17
CQD/g-C_3N_4 nanosheets	20% methanol solution 10 mg catalyst	1.4% (405 nm)	18
g-C_3N_4 nanotubes	3 wt% Pt co-catalyst 10% TEOA solution 10 mg catalyst	6.8% (420 nm)	19
N-GQDs/g-C_3N_4	3 wt% Pt co-catalyst 10% TEOA solution 20 mg catalyst	5.25% (420 nm)	20
VOPc/g-C_3N_4	1 wt% Pt co-catalyst 10% TEOA solution 50 mg of g-C_3N_4+ 2 mg of VOPc	6.29% (420 nm)	21
g-C_3N_4/FcDA	1 wt% Pt co-catalyst 10% TEOA solution 50 mg of g-C_3N_4+ 2 mg of FcDA	7.02% (420 nm)	22
CGT-H_2	2 wt% Pt co-catalyst 10% TEOA solution 10 mg catalyst	4.61% (420 nm)	***This work***

The external quantum efficiency (EQE) have been determined using the follow equation:

$$EQE = \frac{the\ number\ of\ reacted\ electrons}{the\ number\ of\ incident\ photons} \times 100\%$$

Where the number of reacted electrons can be used for the molecule of H_2 evolution, and the number of incident photons is the photons number reaching the surface of catalysts. The H_2 generation rate was measured in the same reaction system as predicted in the experimental section. In addition, photocatalysts were irradiated with monochromatic light generated by equipping with a bandpass filter (420 nm). The numbers of photons were obtained according to the follow equation

$$N = \frac{E\lambda}{hc}$$

Where E, λ, h and c are the light intensity, wavelength, Planck constant and velocity of light, respectively.

In our work, EQE is calculated using the follow equation:

$$N = \frac{E\lambda}{hc} = \frac{40.5 \times 10^{-3} \times 3600 \times 420 \times 10^{-9}}{6.626 \times 10^{-34} \times 3 \times 10^{8}} = 3.08 \times 10^{20}$$

$$EQE = \frac{the\ \ number\ \ of\ \ reacted\ \ electrons}{the\ \ number\ \ of\ \ incident\ \ photons} \times 100\%$$

$$= \frac{2 \times 6.02 \times 10^{23} \times 11.8}{3.08 \times 10^{20}} \times 100\% = 4.61\%$$

References

1. J. Wang, G. Wang, X. Wang, Y. Wu, Y. Su and H. Tang, *Carbon*, 2019, **149**, 618-626.
2. L. Chen, X. Zhou, B. Jin, J. Luo, X. Xu, L. Zhang and Y. Hong, *Int. J. Hydrogen Energy*, 2016, **41**, 7292-7300.
3. X. Wei, C. Shao, X. Li, N. Lu, K. Wang, Z. Zhang and Y. Liu, *Nanoscale*, 2016, **8**, 11034-11043.
4. R. Zhong, Z. Zhang, H. Yi, L. Zeng, C. Tang, L. Huang and M. Gu, *Appl. Catal. B: Environ.*, 2018, **237**, 1130-1138.
5. J. Ma, X. Tan, T. Yu and X. Li, *Int. J. Hydrogen Energy*, 2016, **41**, 3877-3887.
6. J. Wang, J. Huang, H. Xie and A. Qu, *Int. J. Hydrogen Energy*, 2014, **39**, 6354-6363.
7. H. Y. Hafeez, S. K. Lakhera, S. Bellamkonda, G. R. Rao, M. V. Shankar, D. W. Bahnemann and B. Neppolian, *Int. J. Hydrogen Energy*, 2018, **43**, 3892-3904.
8. P. Devaraji and C. S. Gopinath, *Int. J. Hydrogen Energy*, 2018, **43**, 601-613.
9. M. A. Alcudiaramos, M. O. Fuenteztorres, F. Ortizchi, C. G. Espinosagonzalez, N. Hernandezcomo, D. S. Garciazaleta, M. K. Kesarla, J. G. Torrestorres, V. Collinsmartinez and S. Godavarthi, *Ceram. Int.*, 2020, **46**, 38-45.
10. X. Zhong, M. Jin, H. Dong, L. Liu, L. Wang, H. Yu, S. Leng, G. Zhuang, X. Li and J.-g. Wang, *J. Solid State Chem.*, 2014, **220**, 54-59.
11. C. Han, Y. Wang, Y. Lei, B. Wang, N. Wu, Q. Shi and Q. Li, *Nano Res.*, 2015, **8**, 1199-1209.
12. L. Kong, X. Zhang, C. Wang, J. Xu, X. Du and L. Li, *Appl. Surf. Sci.*, 2018, **448**, 288-296.
13. N. Guo, Y. Zeng, H. Li, X. Xu, H. Yu and X. Han, *J. Hazard. Mater.*, 2018, **353**, 80-88.
14. M. Huang, J. Yu, Q. Hu, W. Su, M. Fan, B. Li and L. Dong, *Appl. Surf. Sci.*, 2016, **389**, 1084-1093.
15. X. Han, L. An, Y. Hu, Y. Li, C. Hou, H. Wang and Q. Zhang, *Appl. Catal. B: Environ.*, 2020, **265**, 118539.
16. Y. Xiao, G. Tian, W. Li, Y. Xie, B. Jiang, C. Tian, D. Zhao and H. Fu, *J. Am. Chem. Soc.*, 2019, **141**, 2508-2515.
17. W. Che, W. Cheng, T. Yao, F. Tang, W. Liu, H. Su, Y. Huang, Q. Liu, J. Liu, F. Hu, Z. Pan, Z. Sun and S. Wei, *J. Am. Chem. Soc.*, 2017, **139**, 3021-3026.
18. X. Xia, N. Deng, G. Cui, J. Xie, X. Shi, Y. Zhao, Q. Wang, W. Wang and B. Tang, *Chem. Commun.*, 2015, **51**, 10899-10902.
19. Z. Mo, H. Xu, Z. Chen, X. She, Y. Song, J. Wu, P. Yan, L. Xu, Y. Leia, S. Yuan and H. Li, *Appl. Catal. B: Environ.*, 2018, **225**, 154-161.
20. J.-P. Zou, L.-C. Wang, J. Luo, Y.-C. Nie, Q.-J. Xing, X.-B. Luo, H.-M. Du, S.-L. Luo and S. L. Suib, *Appl. Catal. B: Environ.*, 2016, **193**, 103-109.
21. Y. Liu, L. Ma, C. Shen, X. Wang, X. Zhou, Z. Zhao and A. Xu, *Chin.J. Catal.*, 2019, **40**, 168-176.

22. Y.-N. Liu, X. Zhou, C.-C. Shen, Z.-W. Zhao, Y.-F. Jiang, L.-B. Ma, X.-X. Fang, Z. Akif, T.-Y. Cheag and A.-W. Xu, *Catal. Sci. Technol.*, 2018, **8**, 2853-2859.